Autonomous Multi-MAV Localization of Ionizing Radiation Sources Using Miniature Compton Cameras

Michal Werner[1], Tomáš Báča[1], Petr Štibinger[1],
Daniela Doubravová[2], Jaroslav Šolc[3], Jan Rusňák[3], and Martin Saska[1]

***Abstract*— A novel method for autonomous localization of multiple sources of gamma radiation using a group of Micro Aerial Vehicles (MAVs) is presented in this paper. The method utilizes an extremely lightweight (44 g) Compton camera MiniPIX TPX3. The compact size of the detector allows for deployment onboard safe and agile small-scale Unmanned Aerial Vehicles (UAVs). The proposed radiation mapping approach fuses measurements from multiple distributed Compton camera sensors to accurately estimate the positions of multiple radioactive sources in real time. Unlike commonly used intensity-based detectors, the Compton camera reconstructs the set of possible directions towards a radiation source from just a single ionizing particle. Therefore, the proposed approach can localize radiation sources without having to estimate the gradient of a radiation field or contour lines, which require longer measurements. The instant estimation is able to fully exploit the potential of highly mobile MAVs. The radiation mapping method is combined with an active search strategy, which coordinates the future actions of the MAVs in order to improve the quality of the estimate of the sources' positions, as well as to explore the area of interest faster. The proposed solution is evaluated in simulation and real-world experiments with multiple Cesium-137 radiation sources.**

I. INTRODUCTION

The fast localization of sources of ionizing radiation is a critical task for public safety. UAVs equipped with the appropriate sensors present a viable solution for such a task. The UAVs are able to not only speed up the inspection process, but to replace human workers in hazardous environments, thereby limiting the risk of exposure to harmful radiation imperceptible by human senses. Recent advancements in the field of mobile robotics and sensory equipment have opened new possibilities in the remote sensing of ionizing radiation. We present a radiation mapping method that exploits the benefits and operability of small-scale UAVs equipped with miniature direction-based radiation detectors.

Remote sensing of ionizing radiation is typically done using intensity-based detectors. The use of sensors measuring particle flux at a given position requires scanning the entire area [1], [2], estimating the contour lines [3], [4] or the gradient [5] of the radiation field. The stochastic nature of nuclear fission makes the dosimetric measurements noisy, which needs to be compensated for either by the size of the detector (increased sensitivity) or by acquiring the measurements for a sufficiently long time. Highly sensitive detectors weighing several kilograms must be carried by platforms with a sufficient payload capacity [1], [6], which limits their operability as they are not able to fly close to obstacles, humans, or in cluttered environments. Using miniaturized dosimeters requires longer acquisition times (to record a sufficient number of interactions), which slows down the movement of the UAV and does not fully exploit its potential.

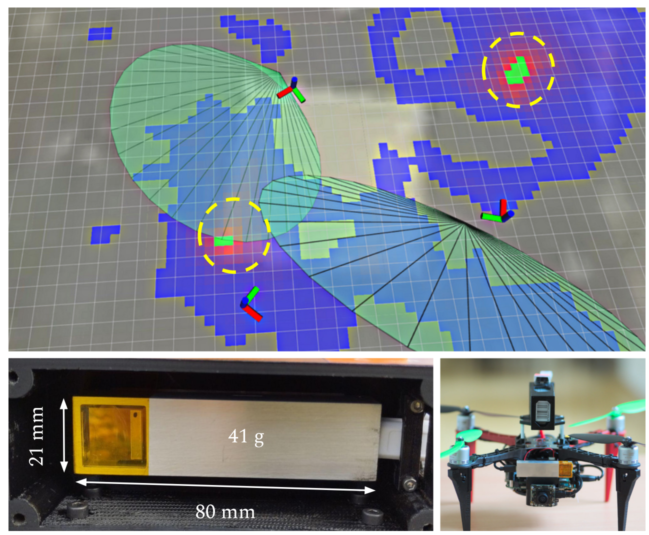

Fig. 1: Estimate of the radioactive hotspots (yellow circles) generated from the Compton measurements (green cones) by the proposed method in a real-world experiment (top). The estimation method builds on a small and lightweight Compton camera (bottom left) that can be deployed onboard sub-1 kg MAVs with onboard processing (bottom right).

Our approach builds on the miniature Compton camera, which belongs to the direction-based class of detectors. A single gamma particle interacting with the matter of the detector in the form of the Compton scattering effect [7] allows us to reconstruct a set of possible directions towards the radioactive source. The event-based nature of the measurements is beneficial, as the MAV is able to keep flying at an arbitrary speed without needing to stop or otherwise constrain its motion. We present a method that fuses the Compton measurements in order to identify multiple sources of ionizing radiation located within the area. We utilize the lightweight and compact MiniPIX TPX3 (Minipix) Compton camera (weighing only 44 g with dimensions $80 \times 21 \times 14$ mm). Thanks to its compactness, the Minipix Compton camera can be mounted onboard agile and lightweight MAVs. The lower effective volume of gamma-absorbent material in the miniature detector is compensated

[1]Authors are with the Faculty of Electrical Engineering, Czech Technical University in Prague, Technická 2, Prague 6, wernemic@fel.cvut.cz.
[2] Authors are with Advacam s.r.o., U Pergamenky 12, 170 00, Prague.
[3] Authors are with Czech Metrology Institute, Okruzni 31, 638 00, Brno.

for, as the small and lightweight MAVs are able to fly closer to possible radiation sources when compared to bulky UAVs or unmanned helicopters. In contrast to intensity-based detectors, the speed of the MAV does not influence the quality of measurements obtained by the onboard Compton event camera. We can, therefore, fully exploit the potential of small and agile MAVs capable of reacting to the newly obtained measurements. Furthermore, the localization process is sped up by the deployment of a team of MAV simultaneously measuring in different locations and the coordination of their actions. We present a novel solution for onboard real-time Compton-camera-based radiation mapping, combined with an active search strategy that guides the MAVs' future actions based on previous measurements. The method was evaluated in simulation, as well as in real-world experiments.

A. Related work

A Compton camera as a direction-based radiation sensor was utilized in the following contributions. Sato et al. [8] presented a large multi-layer Compton camera mounted on a crawler robot moving in one direction. Outdoor radiation imaging using a two-layer Compton camera weighing $1.5\,\mathrm{kg}$ mounted on a drone following a predefined path was presented in [9]. Therein, the Compton measurements were projected onto a 3D map, but all measurements were processed offline. Cong et al. [10] showed a single source localization method in 3D for Compton measurements based on the back projection of cones in the image space. The Maximum Likelihood Expectation Maximization (MLEM) method for Compton measurements reconstruction was originally developed for nuclear imaging in medicine [11]. Authors of [12] presented an offline localization of a single simulated source using the MLEM method for a ground robot equipped with a two-layer Compton camera. However, the authors do not model the sensitivity of detection, which is crucial for the accurate autonomous localization of multiple sources distributed in the area. Vettel et al. [13] presented 3D source localization using the MLEM method and a multilayer Compton camera weighing several kilograms. The search space was restricted to the surface of obstacles obtained by the 3D mapping method. Unlike our solution, all the data were processed offline. In [14], the authors fuse the Minipix Compton camera measurements from multiple UAV with a Linear Kalman Filter (LKF) to localize a single (static or moving) source. Compared to all of the works mentioned above, we present a solution that can localize any number of compact or distributed radiation sources by deploying multiple agile and small MAVs equipped with lightweight and compact Compton cameras.

B. Contribution

This work presents a novel method for the autonomous localization of multiple ionizing radiation sources by a group of MAVs carrying miniature Minipix Compton cameras onboard. In particular, we solve the task of online radiation mapping from Compton measurements by utilizing the maximum-likelihood method and modeling the statistical properties of the single-layer Compton camera (Section III-B). We introduce a simplified model for cone projection (Section III-D) and a memory-efficient representation of detection sensitivity (Section III-C). Therefore, we make the reconstruction method tractable for onboard online estimation in real-world scenarios. As a minor contribution, we combine the radiation mapping method with an active search strategy (Section IV) and demonstrate in both simulation and real-world experiments.

II. PRELIMINARIES

A. Compton measurements

The Compton camera uses the Compton scattering effect [7] to reconstruct the set of possible directions from which the ionizing particle could have reached the sensor. The Compton camera is typically composed of two detectors: a *scatterer* and an *absorber*. The incident photon with energy E_0 first interacts with the *scatterer* where the Compton scattering occurs. An electron with energy E_1 is a bi-product of the interaction, which is immediately captured by the *scatterer*, and its position $\mathbf{x}_1$ and measured energy are recorded. A second product of the interaction, a lower energetic photon with energy E_2, is scattered at a (Compton) angle β. The scattered photon is then absorbed by the *absorber*. The absorbed energy E_2 and the position of the interaction $\mathbf{x}_2$ are measured and recorded. According to [7], the scattering angle β can be reconstructed (following [15]) as:

$$\beta = \cos^{-1}\underbrace{\left(1 + m_e c^2 \left(\frac{1}{E_1 + E_0} - \frac{1}{E_0}\right)\right)}_{B}, \qquad (1)$$

where m_e is is the electron rest mass, c is the speed of light in a vacuum, and $0 < B < 1$. Since the Compton scattering is a symmetrical phenomenon, the set of possible directions of incoming particles forms the surface of a cone. The conical surface (denoted as a Compton cone) is parametrized by the cone axis $\mathbf{a} = \mathbf{x}_2 - \mathbf{x}_1$, the Compton scattering angle β, and the origin of the cone. The simplified geometry is illustrated in Figure 2. More technical details related to the Minipix sensor operation are provided in [15].

B. Problem definition

$\mathbf{x}$, $\|\mathbf{x}\|$	vector in 3D, Euclidean norm of $\mathbf{x}$
$\hat{\mathbf{s}} = (\mathbf{s}, \alpha_0, \alpha_1, \alpha_2)$	oriented sensor pose in 3D
$\tilde{\mathbf{c}}_i = (\hat{\mathbf{s}}_i, \mathbf{a}_i, \beta_i)$	Compton cone with sensor pose $\hat{\mathbf{s}}$, cone-axis vector $\mathbf{a}$, and scattering angle β
$\mathbf{m}_j \in \mathcal{M}$	map position with index $j \in \{1, \ldots, J\}$
$\mathbf{T} \in \mathbb{R}^{I \times J}$, $\mathbf{s} \in \mathbb{R}^J$	system matrix, sensitivity vector
$\boldsymbol{\lambda} \in \mathbb{R}^J$	vector of hidden parameters

TABLE I: Mathematical notation and notable symbols.

As the UAVs fly through the environment, each recorded Compton camera measurement $\tilde{\mathbf{c}}_i = (\hat{\mathbf{s}}_i, \mathbf{a}_i, \beta_i)$ is parameterized by the sensor pose $\hat{\mathbf{s}}$ at the time the measurement was taken, the cone-axis vector $\mathbf{a}$ and the scattering angle β. The Compton cones are indexed with $i \in \{1, \ldots, I\}$, where I is the number of Compton cones recorded by all the UAVs until the current time. The trajectories of the UAVs are sampled with a time period Δt producing viewpoints $\hat{\mathbf{v}}_v$, where $v \in \{1, \ldots, V\}$ and V denotes the total number of viewpoints collected until the current time. The area of interest, where the sources of ionizing radiation might be located, is discretized into J discrete bins with resolution r. Each of the bins is represented by its center position $\mathbf{m}_j$ and indexed with $j \in \{1, \ldots, J\}$, as illustrated in Figure 2. In this paper, we assume that the sources of ionizing radiation are located somewhere on the terrain's surface. Any voxelized 3D map representation (such as an Octomap) can be used as the set $\mathcal{M}$.

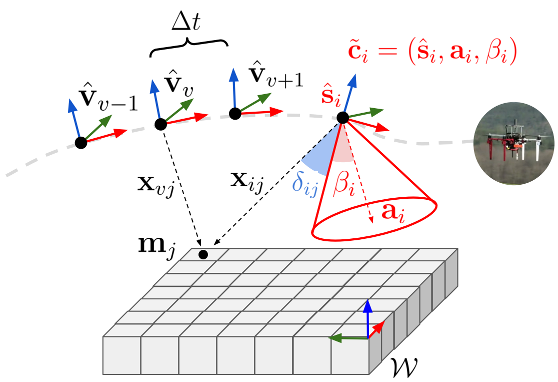

Fig. 2: Compton camera produces Compton cones $\tilde{\mathbf{c}}_i = (\hat{\mathbf{s}}_i, \mathbf{a}_i, \beta_i)$ parameterized by the cones' origin, axis, and the Compton angle, respectively. As the MAV flies through the environment, the viewpoints $\hat{\mathbf{v}}$ are sampled. The area of possible source positions $\mathcal{M}$ is discretized into J cells, where each cell is represented by its center position $\mathbf{m}_j$.

III. RADIATION MAPPING METHOD

A. Maximum likelihood estimation

For designing the radiation mapping approach, we take inspiration from the Maximum Likelihood Expectation Maximization (MLEM) iterative estimation method, which was originally proposed for nuclear medicine applications [11]. We assume that the number of ionizing particles emitted from the position $\mathbf{m}_j$ is a discrete random variable following a Poisson distribution with the expected value λ_j. Every map cell $\mathbf{m}_j$ is a possible radiation source and, therefore, the vector of the unknown parameters $\boldsymbol{\lambda} \in \mathbb{R}^J$ to be estimated is defined as $\boldsymbol{\lambda} = [\lambda_1, \ldots, \lambda_J]$. We further define the matrix $\mathbf{T} \in \mathbb{R}^{I \times J}$ (referred to in the literature as the system matrix) with elements

$$t_{ij} = P(\text{detected in } i | \text{emitted from } j). \tag{2}$$

In other words, t_{ij} represents the probability that we observe the measurement i given that a radioactive particle that caused the measurement i has been emitted from position $\mathbf{m}_j$. Since the measured data are not complete (not every emitted particle reaches the detector and is detected), we define the sensitivity of detection $\mathbf{s} \in \mathbb{R}^J$ with the elements:

$$s_j = P(\text{detected} | \text{emitted from } j), \tag{3}$$

which models the chance that a particle emitted from j is detected by any of the detectors onboard the MAVs. In other words, the sensitivity of detection can be interpreted as the coverage of the area (which is useful for the active search strategy) and enables the accurate localization of multiple radiation sources with different emission activities.

The MLEM algorithm estimates the $\boldsymbol{\lambda}$ at every map position j by maximizing the likelihood of measured data. The likelihood cannot be maximized directly. Therefore, it utilizes the Expectation Maximization (EM) algorithm [16]. One iteration of the MLEM algorithm is defined as

$$\lambda_j^{[l]} = \frac{\lambda_j^{[l-1]}}{s_j} \sum_{i \in \{1,\ldots,I\}} \frac{t_{ij}}{\sum_{k \in \{1,\ldots,I\}} t_{ik} \lambda_k^{[l-1]}}, \tag{4}$$

where l is the current iteration, λ_j is the unknown hidden parameter to be estimated, t_{ij} is an element of the system matrix, and s_j is the sensitivity of detection. To use the MLEM method, we need to model the sensitivity vector $\mathbf{s}$ and system matrix $\mathbf{T}$, which is dependent on the particular sensor device and application. The computation speed is the key factor for running the MLEM algorithm online during the search. Unlike in medical applications where the source-detector distance is low ($\leq 1\,m$), data is processed offline, and the number of measurements is high, we need to make reasonable simplifications to speed up the reconstruction process.

B. Modeling the sensor properties

The probabilistic approach requires modeling equations (2) and (3). The probability of Compton scattering and other particle interactions largely depends on the intersection length between the particle trajectory and the Cadmium Telluride (CdTe) block. Using a Monte Carlo simulation, we model the probability of a Compton measurement caused by a particle approaching the Minipix detector from a certain direction. Although the analytical methods for multi-layer Compton cameras exist, it is difficult to model all the underlying particle interactions inside the Compton camera accurately, as well as unnecessary for the given application. The simulated sources are placed on a sphere with a radius of $1\,\mathrm{m}$ around the detector (the air attenuation is not taken into consideration). Each source position is parameterized with polar angles ϕ, θ as shown in Figure 3a. Every simulated source emits 10^7 particles in all directions. We count the particles emitted from the simulated source towards the visible detector surface that causes interactions resulting in successful Compton measurements. The details of the simulator can be found in [15]. The estimated probability is stored in a lookup table $\mathrm{L}(\phi, \theta)$. For any pair of polar angles $\phi_{querry}, \theta_{qeurry}$, the lookup table returns the stored probability of Compton scattering associated with the nearest ϕ, θ precomputed pair. The simulation results for Cesium-137 are illustrated in Figure 3b. We notice that the direction sensitivity is nearly uniform w.r.t. different angles for Cesium-137, despite the uneven geometry of the detector. Although the particle emitted towards the side of the detector ($\theta \approx \frac{\pi}{2}$) has a lower chance of hitting the detector surface when compared to the particle emitted towards the front of the detector $\phi \approx \frac{\pi}{2}, \theta \approx 0$, the longer intersection with the CdTe block increases the chance of a Compton measurement.

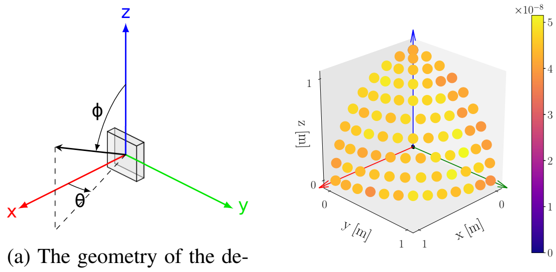

(a) The geometry of the detector and polar coordinates

(b) p(cone) for Cs-137

Fig. 3: Monte Carlo simulation showing the probability of Compton detections at various sensor orientations (i.e., relative positions of the source) with respect to the detector's geometry.

C. Sensitivity estimation

The sensitivity of the detection s_j estimates the chance that a particle emitted at position $\mathbf{m}_j$ has been recorded by the Compton camera onboard the MAVs. First, we model the sensitivity of detection for the viewpoint $\hat{\mathbf{v}}_v$ and map position $\mathbf{m}_j$ pair as:

$$s_{jv} = e^{-(\mu \|\mathbf{m}_j - \mathbf{v}_v\|)} \frac{\mathrm{L}(\phi_{jv}, \theta_{jv})}{\|\mathbf{m}_j - \mathbf{v}_v\|^2}, \tag{5}$$

where μ is the linear attenuation coefficient ($\approx 0.01\,\mathrm{m}^{-1}$ for $622\,\mathrm{keV}$ photons in the air), ϕ_{jv}, θ_{jv} are the polar coordinates determining the relative position of $\mathbf{m}_j$, and the sensor position $\hat{\mathbf{v}}_v$. The sensitivity of detection $s^{[t+1]}$ at time $[t+1]$ is computed as follows:

$$s_j^{[t+1]} = s_j^{[t]} + \sum_{v \in V^{[t:t+1]}} s_{jv} \Delta_v, \tag{6}$$

where the sum $\sum_{v \in V^{[t:t+1]}}$ iterates over all newly processed viewpoints between time t and $t{+}1$. The term $\Delta_v = t_v - t_{v+1}$ expresses the time difference between two consecutive viewpoints. This formulation allows online computation during the flight without extra memory requirements.

D. The system matrix

The system matrix represents the projection of Compton cones to $\mathcal{M}$. The elements t_{ij} are computed as:

$$t_{ij} = e^{-(\mu \|\mathbf{m}_j - \mathbf{s}_i\|)}\ \mathrm{h}(\delta_{ij}) \frac{\mathrm{L}(\phi_{ij}, \theta_{ij})}{\|\mathbf{m}_j - \mathbf{s}_i\|^2}, \tag{7}$$

where μ is the linear attenuation coefficient of the environment ($\approx 0.01\,\mathrm{m}^{-1}$ for $622\,\mathrm{keV}$ photons), ϕ_{ij}, θ_{ij} are the polar coordinates determining the relative position of $\mathbf{m}_j$ and the sensor position $\hat{\mathbf{s}}_i$, $h(\delta_{ij})$ is the projection function, and δ_{ij} is the angle difference (see Figure 2). The projection function

$$\mathrm{h}(\delta_{ij}) = e^{-\frac{1}{2}\left(\frac{\delta_{ij}}{\sigma}\right)^2} \tag{8}$$

projects the cone to $\mathcal{M}$ and models uncertainty in the Compton angle estimation.

IV. MULTIROBOT SEARCH STRATEGY

An important part of the proposed radiation mapping method is a novel active search strategy for a group of autonomous MAVs equipped with Compton cameras. The proposed strategy plans the future movement of the MAVs to increase the information gain and take advantage of the MAVs' mobility. We assume that the communication between MAVs is available and utilize a centralized approach, where one drone plans the future actions for all MAVs. We are aware that many different strategies might be designed based on different robotic missions or required optimality criteria. In this paper, we focus on exploiting the advantages of direction-based radiation sensors in practice and present an efficient solution to the autonomous search for radiation sources. Previous works [14], [5] show that an active search strategy is beneficial compared to extensive exploration of the whole area following a predefined path. Further, an online method can speed up the search process, find the sources faster, and compensate for the effect of less accurate measurements, noise, and background radiation. The task can be divided into two subtasks: **exploration** — visiting areas where no measurements have been collected yet and where an undiscovered ionizing radiation source might be present, and **exploitation** — flying closer to the previously estimated source position to either collect more measurements and make the localization more precise, or to disprove the presence of a radiation source in that location.

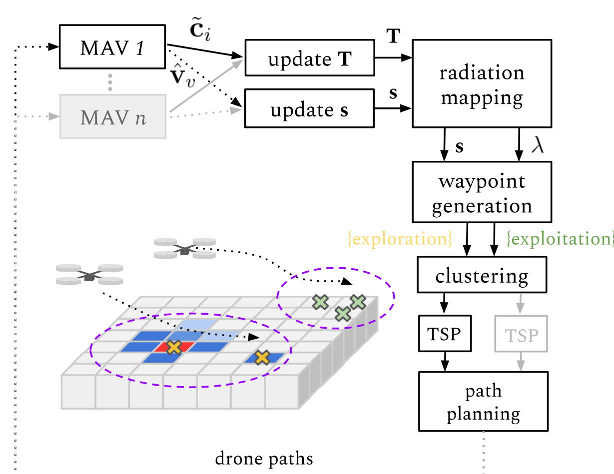

Fig. 4: The search strategy pipeline. The future waypoints for the MAVs are generated based on $\mathbf{s}$ (exploration) and $\boldsymbol{\lambda}$ (exploitation). The waypoints are assigned to individual MAVs by dividing them into clusters based on their spatial position (purple circles). The ordering of waypoints is determined using the sequencing method (TSP). Finally, the pipeline outputs non-colliding paths.

The search strategy is illustrated in Figure 4. The **waypoint generation** method generates waypoints based on the most recent estimate of $\boldsymbol{\lambda}$ and s.The point $\mathbf{m}_j$ is taken as the *exploration* waypoint if $\mathbf{s}_j < s_{min}$, where s_{min} is a preset threshold specifying the minimum required chance that a particle emitted at this position has been detected by the MAVs. The *exploration* waypoints $\mathbf{w_s}$ are then clustered using the K-Means method to reduce their number. For the *exploitation* waypoints $\mathbf{w}_{\boldsymbol{\lambda}}$, we use local maxima in the map $\mathcal{M}$ based on the latest $\boldsymbol{\lambda}$.

While the waypoints that have not recently been visited by any of the MAV are prioritized, the generated waypoints $\{\mathbf{w}_{\boldsymbol{\lambda}} \cup \mathbf{w}_{\mathbf{s}}\}$ are filtered and assigned to individual MAVs using a **clustering** method. The number of clusters equals the number of MAVs, and each cluster centroid is initialized at the current position of each MAV. The waypoints assigned to each MAV are then ordered into an optimal sequence using a Travelling salesman problem (TSP) solver, where the sequence always starts at the current position of the MAV and ends in any of the assigned waypoints. Finally, the **path planning** method plans non-colliding paths for all MAVs, visiting all assigned waypoints using the A* algorithm.

V. EXPERIMENTS

A. Real-world experiment

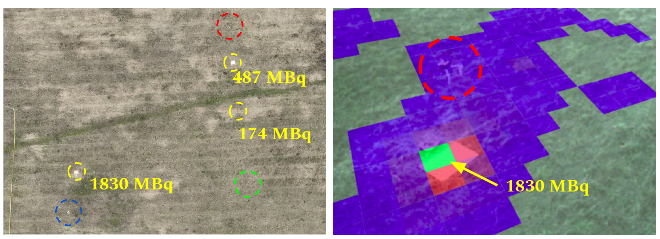

(a) The UAVs (red/green/blue) and radiation sources (yellow) during the experiment ($t = 32\,\mathrm{s}$).

(b) Estimated radiation intensity around the $1830\,\mathrm{MBq}$ radiation source with UAV above. ($t = 520\,\mathrm{s}$)

Fig. 5: The real-world experiment with Cs-137 radiation sources.

We present the real-world experiment as a proof of concept and validation of the proposed method. The system was tested with three UAVs in an open field 50×70 m where three Cesium-137 sources with emission activity $1830, 487, 174$ MBq were present, as shown in Figure 5. The estimated emission activity of the radiation sources and trajectories of the UAVs are shown in Figure 6.

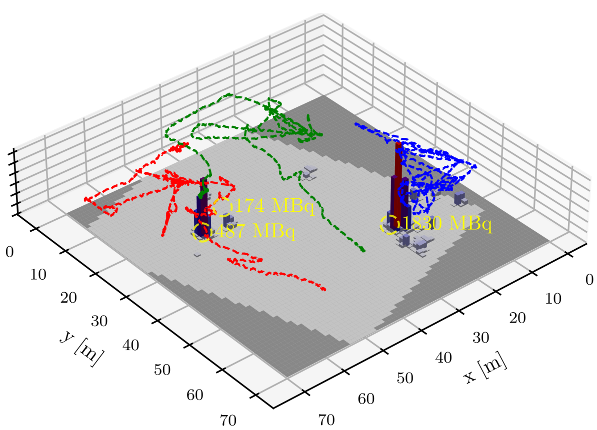

Fig. 6: The result of the real-world search mission with three UAVs after $240\,\mathrm{s}$. The estimated emission intensity $\boldsymbol{\lambda}$ is shown as the 3D bars (grey-blue-red colour scale), the unexplored area ($s_j < s_{min}$) is shown in light green, and the MAVs trajectories are depicted as dashed lines. The ground truth positions of the radiation sources are shown with yellow dashed circles.

Two of three Cesium-137 were localized within $108\,\mathrm{s}$. After collecting more measurements, the estimates converged to their true position while correctly evaluating their relative emission activity. The third least active $174\,\mathrm{MBq}$ source remained undiscovered due to its low emission activity, which shows the detection limits of the proposed system. The experiment demonstrates the ability to localize multiple radiation sources of different emission activity in a large, open-space area. The proposed method should be further tested with additional radiation sources and with more agile MAV capable of flying up to $8\,\mathrm{m\,s^{-1}}$ or more, as these were unavailable at the time of experimentation. The video from the experiment is available at https://mrs.felk.cvut.cz/iros-compton-2024.

B. Simulation

Conducting real-world experiments with real ionizing radiation sources is complicated due to logistical reasons requiring coordination between multiple institutions, as well as legal restrictions. Consequently, the real-world experiments had to be performed within a short window of several hours. Therefore, the proposed method was also tested in the realistic MRS multirotor simulator [17] with simulated ionizing radiation [15]. The progress of one simulated experiment with 3 MAVs (with maximum speed $8\,\mathrm{m\,s^{-1}}$) and 5 simulated sources is shown in Figure 7.

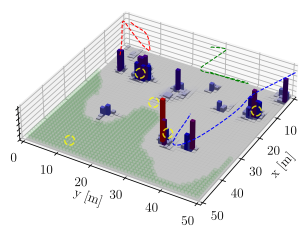

(a) $t = 15\,\mathrm{s}$

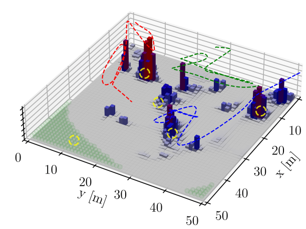

(b) $t = 30\,\mathrm{s}$

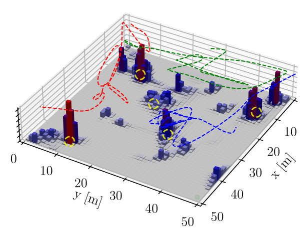

(c) $t = 45\,\mathrm{s}$

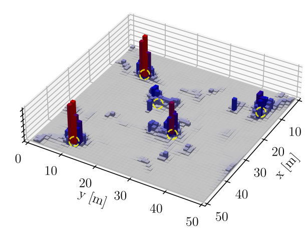

(d) $t = 100\,\mathrm{s}$

Fig. 7: The progress of one simulated search mission with three MAVs. The estimated emission intensity $\boldsymbol{\lambda}$ is shown as the 3D bars (grey-blue-red colour scale). The unexplored area ($s_j < s_{min}$) is shown in light green, and the MAVs' trajectories are depicted as dashed lines. The map resolution r is $0.5\,\mathrm{m}$. The ground truth positions of the $2\,\mathrm{GBq}$ sources are shown with yellow circles.

The simulated experiment was repeated 10 times and the localization error (the distance between the ground truth position and nearest estimated source) is shown in Figure 8. The proposed search strategy converges to the true source positions, with the Root Mean Square Error (RMSE) decreasing below $2\,\mathrm{m}$ precision threshold after $220\,\mathrm{s}$. All simulated sources are localized within $2\,\mathrm{m}$ precision after $300\,\mathrm{s}$. The effectiveness of the presented search strategy is demonstrated by comparison with a predefined zigzag search pattern (also repeated 10 times), where the search area is divided into three equal parts, and each part is covered by an MAV following a zigzag trajectory with a $2\,\mathrm{m}$ lateral step and a maximum flight speed of $8\,\mathrm{m\,s^{-1}}$. In comparison, the zigzag search strategy shows slower convergence than our approach because the MAVs following predefined paths do not fly closer to the estimated source positions, resulting in fewer collected measurements and less accurate reconstruction of the radiation sources.

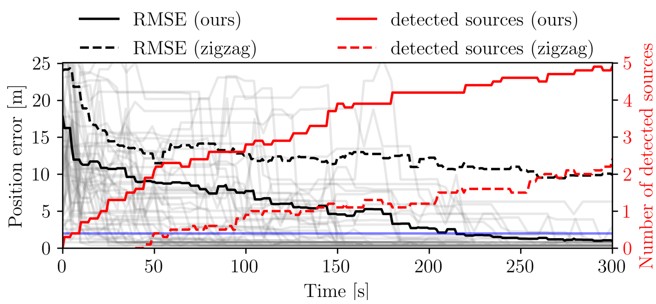

Fig. 8: The localization error for each simulated source for 10 simulated experiments (light grey), RMSE (black) and the average number of the localized sources within $2\,\mathrm{m}$ precision (red). We compare the proposed search strategy (solid line) with a predefined zigzag search pattern (dashed line).

VI. CONCLUSION

In this work, we have presented a novel approach to the autonomous localization of multiple ionizing radiation sources. This was done by using single-layer Compton cameras onboard MAVs working in a team. We have enabled online radiation mapping by modeling the detection sensitivity of the Compton camera, and the reconstructive projection of Compton cones into a volumetric map. Furthermore, we have expanded the capabilities of the maximum likelihood radiation detection method by coupling it with an active search strategy. This strategy leverages the online processing of Compton measurements to plan the future movements of the MAVs. The method has been validated in both simulation and a real-world experiment, demonstrating the system's ability to autonomously detect previously unknown radiation sources, and to improve the quality of source localization during flight.

The proposed method relies heavily on the occurrence of the Compton scattering effect. The data collected from the real-world experiment highlighted that this effect comprises only a small subset of all radiation events captured by the detector. A potential direction for future work involves combining the direction-based Compton camera approach with intensity-based methods. Developing estimation methods that merge the advantages of both could significantly enhance the robots' capabilities in terms of fast and accurate localization of harmful ionizing radiation sources.

ACKNOWLEDGMENTS

This work was funded by CTU grant no SGS23/177/OHK3/3T/13, by the Czech Science Foundation (GAČR) under research project no. 23-07517S and by the European Union under the project Robotics and advanced industrial production (reg. no. CZ.02.01.01/00/22_008/0004590).

REFERENCES

[1] Y. Sanada *et al.*, "Aerial radiation monitoring around the Fukushima Dai-ichi nuclear power plant using an unmanned helicopter," *Journal of Environmental Radioactivity*, vol. 139, pp. 294–299, Jan. 2015.

[2] P. G. Martin *et al.*, "3D unmanned aerial vehicle radiation mapping for assessing contaminant distribution and mobility," *International Journal of Applied Earth Observation and Geoinformation*, vol. 52, pp. 12–19, Oct. 2016.

[3] A. A. Redwan Newaz *et al.*, "UAV-based multiple source localization and contour mapping of radiation fields," *Robotics and Autonomous Systems*, vol. 85, pp. 12–25, Nov. 2016.

[4] J. Han, Y. Xu, L. Di, and Y. Chen, "Low-cost Multi-UAV Technologies for Contour Mapping of Nuclear Radiation Field," *Journal of Intelligent & Robotic Systems*, vol. 70, no. 1, pp. 401–410, Apr. 2013.

[5] F. Mascarich *et al.*, "Autonomous Distributed 3D Radiation Field Estimation for Nuclear Environment Characterization," in *2021 IEEE International Conference on Robotics and Automation (ICRA)*. Xi'an, China: IEEE, May 2021, pp. 2163–2169.

[6] J. Towler *et al.*, "Radiation Mapping in Post-Disaster Environments Using an Autonomous Helicopter," *Remote Sensing, vol. 4, issue 12, pp. 1995-2015*, vol. 4, pp. 1995–2015, Jul. 2012.

[7] A. H. Compton, "A Quantum Theory of the Scattering of X-rays by Light Elements," *Phys. Rev.*, vol. 21, pp. 483–502, 5 1923.

[8] Y. Sato *et al.*, "Radiation imaging using a compact Compton camera mounted on a crawler robot inside reactor buildings of Fukushima Daiichi Nuclear Power Station," *Journal of Nuclear Science and Technology*, vol. 56, pp. 1–8, Feb. 2019.

[9] Y. Sato, S. Ozawa *et al.*, "Remote detection of radioactive hotspot using a Compton camera mounted on a moving multi-copter drone above a contaminated area in Fukushima," *Journal of Nuclear Science and Technology*, vol. 57, no. 6, pp. 734–744, Jun. 2020.

[10] F. Cong *et al.*, "Radioactive source recognition with moving Compton camera imaging robot using Geant4," *Nuclear Instruments and Methods in Physics Research Section A: Accelerators, Spectrometers, Detectors and Associated Equipment*, vol. 953, p. 163108, Feb. 2020.

[11] S. Wilderman *et al.*, "List-mode maximum likelihood reconstruction of compton scatter camera images in nuclear medicine," in *1998 IEEE Nuclear Science Symposium Conference Record. 1998 IEEE Nuclear Science Symposium and Medical Imaging Conference (Cat. No.98CH36255)*, vol. 3, 1998, pp. 1716–1720 vol.3.

[12] D. Kim *et al.*, "3D radiation imaging using mobile robot equipped with radiation detector," in *2017 IEEE/SICE International Symposium on System Integration (SII)*, Dec. 2017, pp. 444–449.

[13] K. Vetter *et al.*, "Gamma-Ray imaging for nuclear security and safety: Towards 3-D gamma-ray vision," *Nuclear Instruments and Methods in Physics Research Section A: Accelerators, Spectrometers, Detectors and Associated Equipment*, vol. 878, pp. 159–168, Jan. 2018.

[14] T. Baca *et al.*, "Gamma Radiation Source Localization for Micro Aerial Vehicles with a Miniature Single-Detector Compton Event Camera," in *2021 International Conference on Unmanned Aircraft Systems (ICUAS)*, Jun. 2021, pp. 338–346.

[15] T. Baca, M. Jilek *et al.*, "Timepix Radiation Detector for Autonomous Radiation Localization and Mapping by Micro Unmanned Vehicles," in *2019 IEEE/RSJ International Conference on Intelligent Robots and Systems (IROS)*. Macau, China: IEEE, Nov. 2019, pp. 1129–1136.

[16] A. P. Dempster *et al.*, "Maximum Likelihood from Incomplete Data via the EM Algorithm," *Journal of the Royal Statistical Society. Series B (Methodological)*, vol. 39, no. 1, pp. 1–38, 1977.

[17] T. Baca *et al.*, "The MRS UAV System: Pushing the Frontiers of Reproducible Research, Real-world Deployment, and Education with Autonomous Unmanned Aerial Vehicles," *Journal of Intelligent & Robotic Systems*, vol. 102, no. 26, pp. 1–28, 05 2021.